Seismicity and tectonics of the South Shetland Islands and Bransfield Strait from a regional broadband seismograph deployment

Stacey D. Robertson Maurice,[1] Douglas A. Wiens, and Patrick J. Shore
Department of Earth and Planetary Sciences, Washington University, St. Louis, Missouri, USA

Emilio Vera
Departmento de Geofisica, Universidad de Chile, Santiago, Chile

LeRoy M. Dorman
Scripps Institution of Oceanography, La Jolla, California, USA

Received 22 January 2003; revised 22 April 2003; accepted 14 May 2003; published 9 October 2003.

[1] We investigate the tectonics of the South Shetland Trench and Bransfield Strait by performing a detailed study of local seismicity. During 1997–1999 we deployed seven land seismometers and 14 ocean bottom seismometers in the South Shetland Island region. The data we obtained indicate a high level of local seismicity (m_b 2–5), and we accurately located ~150 earthquakes. Many of the earthquakes occur at locations and depths indicative of ongoing subduction in the South Shetland trench. A focal mechanism for the largest event in the forearc indicates shallow angle thrusting. The maximum depth of seismicity is ~65 km, but the majority of the events are shallower than 30 km. These seismic results are consistent with recent magnetic, GPS, and multichannel seismic reflection data that suggest continued subduction at a very slow rate. The South Shetland trench thus represents an extreme end-member of hot subduction resulting from slow convergence of young lithosphere, and the absence of intermediate depth earthquakes is consistent with thermal assimilation of the slab at shallow depths. We have located many earthquakes associated with volcanism and rifting in Bransfield Strait. A swarm of events near a submarine volcano suggests current magmatic activity. A normal faulting focal mechanism in the northeastern part of the strait gives evidence of extension. Earthquakes associated with rifting in the northeastern portion of the strait are clustered along well-established rifts, but the seismicity is much more diffuse to the southwest. This observation is consistent with other evidence that extension has propagated from northeast to southwest. *INDEX TERMS:* 7230 Seismology: Seismicity and seismotectonics; 7294 Seismology: Instruments and techniques; 8150 Tectonophysics: Plate boundary—general (3040); 8158 Tectonophysics: Plate motions—present and recent (3040); 9310 Information Related to Geographic Region: Antarctica; *KEYWORDS:* Bransfield Strait, South Shetland Islands, Antarctic Peninsula, seismicity, subduction, back arc rifting

Citation: Robertson Maurice, S. D., D. A. Wiens, P. J. Shore, E. Vera, and L. M. Dorman, Seismicity and tectonics of the South Shetland Islands and Bransfield Strait from a regional broadband seismograph deployment, *J. Geophys. Res.*, *108*(B10), 2461, doi:10.1029/2003JB002416, 2003.

1. Introduction

[2] The South Shetland Island-Antarctic Peninsula region is a geodynamic system undergoing rapid changes in plate motions and configuration. The South Shetland Trench, located just seaward of the South Shetland Islands, is the last surviving segment of a subduction zone that once extended all along the western margin of the Antarctic Peninsula [e.g., *Cande et al.*, 1982]. The tectonic setting in this subduction zone was very unique because the trailing flank of the ridge crests and the overriding lithosphere at the trench were both part of the Antarctic plate. Therefore there was no relative motion between the plates, and ridge-trench collisions caused cessation of subduction at each segment. The subduction zone shortened gradually as segments of the Phoenix spreading ridge (sometimes referred to as the Aluk spreading ridge) collided with the Antarctic margin, and the only remaining ridge segments in Drake Passage became inactive approximately 4 Ma [*Larter and Barker*, 1991]. Subduction at the South Shetland Trench must have slowed or ceased completely at this time. Figure 1 shows the major tectonic elements of this region [after *Barker and Dalziel*, 1983; *Pelayo and Wiens*, 1989].

[1] Now at ExxonMobil Upstream Research Co., Houston, Texas, USA.

0148-0227/03/2003JB002416$09.00

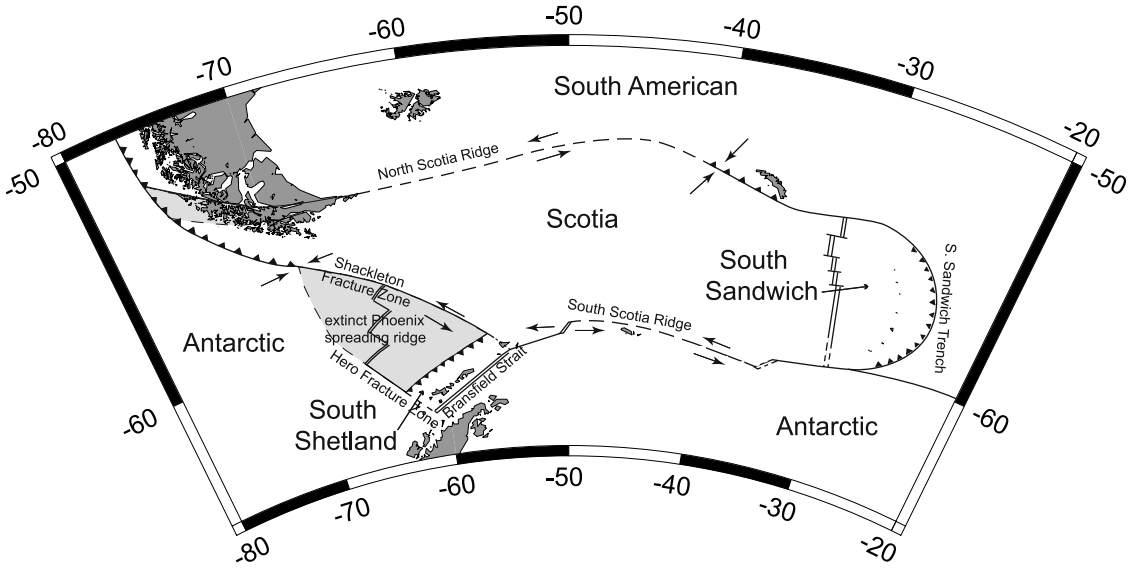

Figure 1. Tectonic map of the Antarctic Peninsula and Scotia Sea region [after *Pelayo and Wiens*, 1989]. Subduction once extended along the entire western margin of the Antarctic Peninsula, but only a small section of the trench remains. The Phoenix spreading ridge ceased spreading at 4 Ma, and rifting was recently initiated in the Bransfield Strait. The shaded zones represent areas of diffuse seismicity.

[3] Although the South Shetland Trench has a morphology similar to that of active trenches [*Maldonado et al.*, 1994], global seismic catalogs show low levels of seismicity and no evidence of the shallow thrust faulting earthquakes that occur in most subduction zones. The main seismological evidence of subduction is one or two earthquakes located at depths greater than would normally be expected in a nonsubduction environment. *Pelayo and Wiens* [1989] located one event at 55 km depth near Smith Island using teleseismic body waveform inversion. This event showed a strike-slip focal mechanism, so they suggested it might have occurred within a subducting plate. However, only one earthquake of that depth has been found, and the teleseismic earthquake analysis was limited to a few larger earthquakes. *Ibanez et al.* [1997] found evidence for earthquakes as deep as 100 km using a tight array of stations on Deception Island, but their depth constraints were limited since the small aperture array was subject to large uncertainties in ray parameter due to possible local structure effects. Seismic recordings at King Sejong station indicate that local earthquakes occur frequently in northern Bransfield Strait, but the locations of many of these events are unknown [*Jin et al.*, 1998]. Thus seismological evidence of subduction and the possible presence of downgoing lithosphere beneath the South Shetland Islands is extremely limited. The absence of seismicity in global catalogs may result from the poor global station distribution for earthquakes in this region; the closest stations for earthquakes in this region have generally been at distances of 20° or more, and the detection threshold may have been close to m_b 5.0 for most of the last 40 years [*Larter*, 2001].

[4] If subduction is still occurring beneath the South Shetland Islands, the subduction rate should be similar to the opening rate of Bransfield Strait, due to the fact that the subducting plate and the overriding plate have no relative motion between them. Several estimates of spreading rate have been made using magnetic anomaly data, including 2.4 cm/yr [*Roach*, 1978; *Barker and Dalziel*, 1983] and 0.9 cm/yr [*Parra and Yanez*, 1988]. However, the magnetic data from the Bransfield Strait are difficult to interpret, and it is not clear whether normal seafloor spreading has developed at this time [*Barker et al.*, 2003]. Preliminary GPS measurements indicate a spreading rate of ~1 cm/yr or slower [*Bevis et al.*, 1999; *Dietrich et al.*, 2001]. This rate would suggest that the South Shetland trench represents an extreme end-member of hot subduction involving slow convergence of young oceanic lithosphere (14 Ma at the southwestern segment to 23 Ma at the northeastern limit of the trench).

[5] Further evidence of back arc extension in Bransfield Strait includes extensional earthquake mechanisms [*Forsyth*, 1975; *Pelayo and Wiens*, 1989], a lineated seafloor with large volcanic constructs [*Gracia et al.*, 1996, 1997; *Keller et al.*, 2002; *Lawver et al.*, 1996], high heat flow [*Nagihara and Lawver*, 1989], and petrologic constraints [*Weaver et al.*, 1979; *Keller et al.*, 1992]. The South Shetland back arc is unique because it may presently be in transition from a rifting regime to a spreading regime [*Barker and Austin*, 1994].

[6] Crustal thickness estimates for Bransfield Strait have been inconsistent [*Ashcroft*, 1972; *Grad et al.*, 1993, 1997], but detailed refraction ocean bottom seismograph (OBS) profiles [*Barker et al.*, 2003] show that the back arc crust is thinning, and that the crustal thickness in Bransfield Basin increases from ~10 km in the central portion to ~14–16 km in the southwest. *Della Vedova* [1999] also performed seismic refraction work near the Antarctic Peninsula and found that the crust in Bransfield Basin is 15–17 km thick and that it becomes markedly thicker southwest of the Hero Fracture Zone. The crust is undergoing extension but new oceanic crust is not forming, and extension is focused in the side of the strait adjacent to the South Shetland Islands, causing physiographic asymmetry in the Strait [*Barker et al.*, 2003].

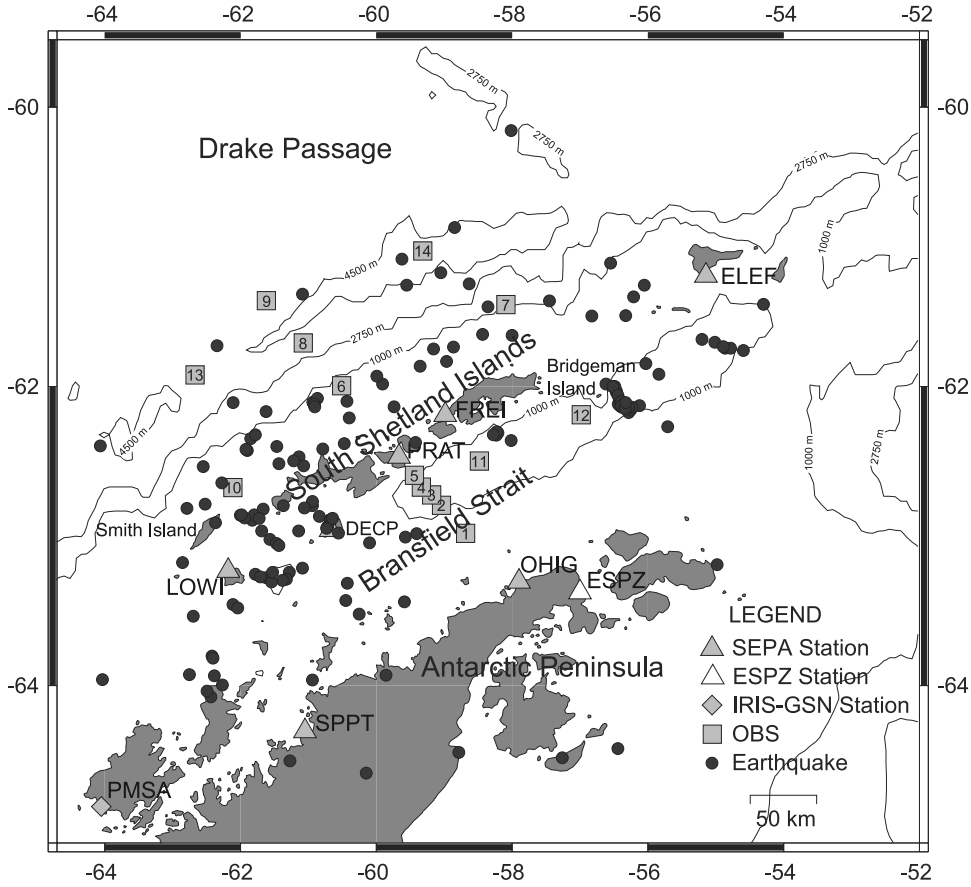

Figure 2. Locations of land stations (triangles and diamond) and OBSs (squares). Earthquake locations determined from the SEPA deployment are shown as circles. The 95% confidence ellipsoids for the locations are small, approximately the size of the circles themselves.

[7] The Seismic Experiment in Patagonia and Antarctica (SEPA) was a 2.5-year deployment of portable broadband seismic instrumentation on the Antarctic Peninsula, South Shetland Islands, and Chilean Patagonia. A corresponding 6-month deployment of ocean bottom seismographs occurred in the Bransfield Strait and South Shetland forearc regions. This new study provides a good data set of locally recorded earthquakes, thus helping to remove the limitations posed by the sparse earthquake data set resulting from the global seismic arrays' poor coverage of South Shetland earthquakes. In this paper we study the local seismicity of the South Shetland Trench and Bransfield Strait in order to better understand the tectonics of the region.

2. Deployment

[8] The Antarctic portion of the SEPA project included seven land stations and 14 ocean bottom seismometers (OBSs) (Figure 2). Each land station consisted of a Streckeisen STS-2 seismometer and a Reftek 24 bit digital acquisition system with GPS timing. Data were recorded continuously at 25 or 40 samples per second on one to four gigabyte magnetic disks. The three stations at Antarctic bases were outfitted with ARGOS state-of-health satellite transmitters to help maintain reliable operation despite their limited access. These transmitters allowed remote monitoring of the status of the instrument, and therefore possible correction of problems at the Antarctic bases through communication with local operators.

[9] The first five Antarctic stations were established on a cruise of the Chilean Naval vessel *Isaza*, sponsored by the Instituto Antartico Chileno (INACH), during January 1997. These stations were serviced and two new stations were constructed during the follow-up cruises of the R/V *Abel-J*, the *Isaza*, the R/V *L. M. Gould*, and the R/V *N. B. Palmer*. Two types of stations were established in the Antarctic, depending on whether the stations were located at inhabited bases or in the field. Three of the sites (Frei, Prat, and O'Higgins) were located at permanent bases operated by branches of the Chilean armed forces. The sensors at these stations were located several hundred meters from the buildings on the base, and the base provided AC power as well as occasional station servicing.

[10] Four other sites (Spring Point and Elephant, Deception, and Low Islands) were located in the field, with no attendants or electric power available. Logistics permitted visits to these sites only once or twice a year during the Antarctic summer. These sites were equipped with power supplies designed by the Lamont Passcal Instrument Center, which used solar power during most of the year, but relied on banks of 18 Carbonaire batteries during the winter months. Some stations operated throughout the entire winter unattended, and the majority of the Antarctic field stations recorded data for about 9 months each year. The field

Table 1. SEPA Station Locations and Installation Periods

Station	Location	Latitude	Longitude	Start Date	End Date
DECP	Deception Island, Antarctica	−62.977	−60.670	Jan. 1997	May 1999
ELEF	Elephant Island, Antarctica	−61.220	−55.139	Jan. 1997	May 1999
PRAT	Prat Base, Greenwich Island, Antarctica	−62.480	−59.664	Jan. 1997	Nov. 2001
FREI	Frei Base, King George Island, Antarctica	−62.195	−58.984	Jan. 1997	Nov. 2001
OHIG	O'Higgins Base, Antarctic Peninsula	−63.321	−57.898	Jan. 1997	Nov. 2001
LOWI	Low Island, Antarctica	−63.247	−62.181	Dec. 1997	May 1999
SPPT	Spring Point, Antarctic Peninsula	−64.295	−61.051	Dec. 1998	May 1999
HAMB	Puerto del Hambre, Chile	−53.614	−70.931	Jan. 1997	present
MILO	Cueva del Milodon, Chile	−51.568	−72.620	Jan. 1997	Nov. 1998
FELL	Fell Ranch, Chile	−52.057	−70.005	Jan. 1997	Nov. 1998
SALM	Skyring, Chile	−52.549	−72.030	Jan. 1997	Nov. 1998
VTDF	Vicuna Ranch, Chile	−54.138	−68.706	Jan. 1997	Nov. 1998

stations were removed during a cruise of the R/V *N.B. Palmer* in May 1999, and the stations at the Chilean bases were removed during a cruise of the R/V *N.B. Palmer* in November 2001. The installation period for each station is shown in Table 1.

[11] During December 1998 through May 1999 we also deployed 14 ocean bottom seismometers (OBSs) of the Office of Naval Research (ONR) type [*Jacobson et al.*, 1991; *Sauter et al.*, 1990]. The primary OBS line is perpendicular to the SEPA array, so the OBS data allowed for more accurate locations of events. Seven of the OBSs were equipped with broadband Precision Measurement Device (PMD) sensors, model 2123, and the other seven used 1 Hz L4 sensors. All OBSs were also equipped with differential pressure gauges [*Cox et al.*, 1984]. The OBS locations are shown in Table 2.

3. Methods

3.1. Earthquake Locations

3.1.1. Preliminary Locations

[12] The local earthquake study extends from 29 January 1997 to 31 May 1998 and 1 December 1998 to 20 May 1999. Few of the stations were operating during June–November 1998, so we did not locate earthquakes during those months. The station at O'Higgins was inoperable from March through July 1997, so during this time we used data from the near-by Argentinean/Italian station, Esperanza (ESPZ). Because of the high level of ice-induced seismic noise, automated earthquake identification algorithms did not work well, and earthquakes were identified by visually scanning the raw records from several stations. Figure 3 shows typical waveforms for one OBS and one land station. Error bounds were assigned to each *P* and *S* arrival based on the clarity of the pick and are indicated with grey shading in Figure 3. *P* and *S* wave arrivals were picked using Datascope [*Quinlan et al.*, 1996], an interactive arrival time picking and location package, and preliminary locations for the earthquakes were determined using the IASPEI91 velocity model [*Kennett and Engdahl*, 1991]. IASPEI91 is a global velocity model, so some improvement of the earthquake locations should be expected using a model developed specifically for this region. However, attempts to locate the events using a previously developed velocity model for the Bransfield Strait [*Grad et al.*, 1993, 1997] resulted in higher arrival time misfits for most earthquakes. We therefore determined that we needed to use a different velocity model, and that it was best to incorporate different structural models for the different tectonic regions to account for lateral heterogeneity.

3.1.2. Final Earthquake Locations

[13] We calculated final earthquake locations using separate structural models for the forearc, South Shetland platform, back arc, and peninsula. The crustal structures of the forearc, South Shetland platform, and back arc were taken from the refraction profiles of *Barker et al.* [2003]. The peninsula crustal structure was taken from receiver function analyses at Palmer station [*Vuan*, 2001; J. Fisher, personal communication, 2002]. The mantle structure for all four models was taken from regional surface wave tomography (A. Vuan, unpublished manuscript, 2002) at depths shallower than 70 km. The velocity values at 35–60 km depth are equivalent to 3% slower than IASPEI91 velocities, and the values at 60–100 km depth are equivalent to 1.5% slower than IASPEI91. Standard IASPEI91 values were used below 100 km. The *P* to *S* velocity ratios of the models were set to the ratios of the corresponding region (crust or mantle) in the IASPEI91 velocity model. The four velocity structures used are shown in Table 3.

[14] Final earthquake locations were obtained using J. Lahr's HYPOELLIPSE location program [*Lahr*, 1999]. Only one structural model was used for each location, and we chose the appropriate model for each event based upon the tectonic region of the preliminary earthquake location.

Table 2. OBS Locations[a]

OBS	Latitude	Longitude	Depth, m	Instrument Type
1	−63.000	−58.681	295	1 Hz L4
2	−62.809	−59.040	1411	1 Hz L4
3	−62.740	−59.182	1426	Precision Measuring Device (PMD) model 2123
4	−62.689	−59.333	1420	1 Hz L4
5	−62.608	−59.434	1275	Precision Measuring Device (PMD) model 2123
6	−62.996	−60.508	1607	1 Hz L4
7[b]	−61.426	−58.090		
8	−61.697	−61.078	4183	Precision Measuring Device (PMD) model 2123
9	−61.400	−61.614	3701	Precision Measuring Device (PMD) model 2123
10	−62.692	−62.110	591	Precision Measuring Device (PMD) model 2123
11	−62.510	−58.475	1627	1 Hz L4
12[b]	−62.194	−56.983		
13	−61.915	−62.669	3988	1 Hz L4
14[b]	−61.045	−59.316		

[a]The OBSs were deployed December 1998 to May 1999.
[b]Indicates instrument that did not record data.

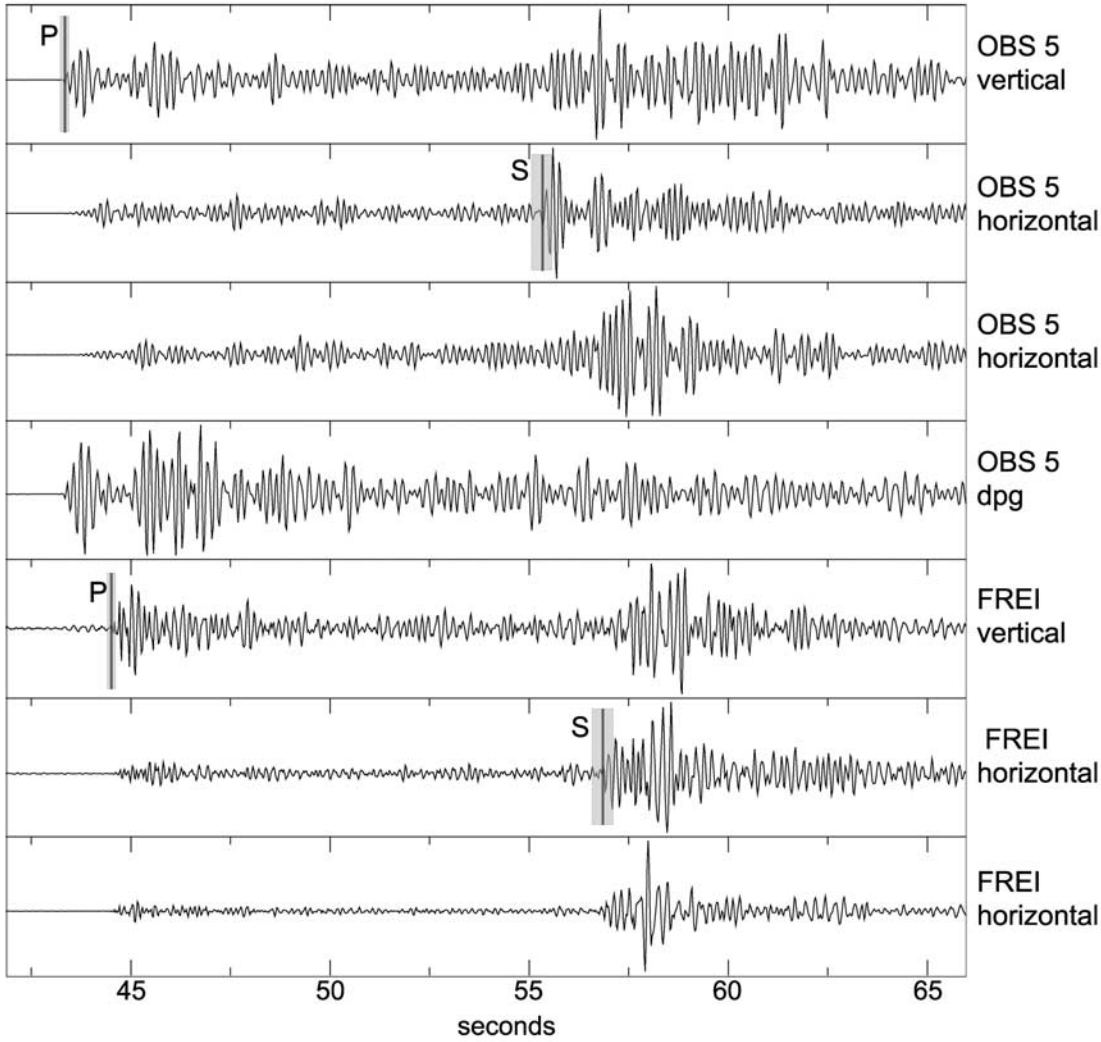

Figure 3. Waveforms recorded by OBS 5 and FREI for a local earthquake on 29 January 1999. The *P* and *S* arrival picks are shown with lines, and the error bounds placed on each pick are shown with grey shading.

Each earthquake in our compilation was located using a minimum of five clear *P* wave or *S* wave arrivals. However, most of the earthquake locations incorporated between 6 and 31 arrivals recorded by 4–16 stations. The earthquakes located during the 6 months of the OBS deployment naturally incorporated more arrival times than those located when only the land stations were operating, and are thus better constrained.

[15] The new locations had lower residual time errors than the preliminary IASPEI91 locations and the solutions were more robust. The locations determined using the new local structural models seldom varied from the original IASPEI91 locations by more than 10 km laterally. The change in earthquake depth with structural models was sometimes significant, but for many of the events the depths were poorly constrained. For the events with well-constrained depths (below), the variation in depth with different structural models was 10 km or less.

[16] After locating the earthquakes we saw that there were two distinct clusters of events in the northeastern portion of Bransfield Strait, one near Bridgeman Island and one south of Elephant Island. Both of these clusters include earthquakes that occurred in rapid succession several times over the course of the deployment. We used a multiple-event relocation program based on the hypocentroidal decomposition algorithm [*Jordan and Sverdrup*, 1981] to calculate relative locations for these events and better constrain the depths, as these events were outside the tight array of seismometers. The swarm near Bridgeman Island contained 24 events located at depths of 12 km or less. The swarm south of Elephant Island contained six events that were all located at ~30 km deep, but the depth of these events are uncertain due to poor station coverage.

3.1.3. Quality Assessment

[17] We used HYPOELLIPSE to classify the earthquake location quality on a scale of A though D. A separate confidence ellipsoid was calculated for the lateral location and the depth, thus giving each earthquake two quality classifications. The scale used to qualify the locations was the same for both the horizontal and vertical directions. If the maximum radius of the 95% confidence ellipsoid for the location was less than 2.6 km, then the earthquake was ranked

Table 3. Velocity Models Used for Earthquake Locations and Focal Mechanisms

Depth, km	V_P	V_S
	Forearc	
0.00	4.50	2.60
2.20	6.30	3.63
8.00	7.00	4.04
19.00	7.10	4.10
24.00	7.50	4.33
35.10	7.85	4.36
40.13	7.86	4.38
60.28	8.01	4.46
80.51	8.04	4.49
100.79	8.19	4.58
121.14	8.25	4.60
141.56	8.33	4.61
162.04	8.41	4.63
182.59	8.50	4.65
203.21	8.56	4.67
213.54	8.63	4.70
234.25	8.74	4.75
255.04	8.84	4.81
275.89	8.95	4.86
296.81	9.05	4.91
317.80	9.16	4.96
338.85	9.27	5.02
359.98	9.38	5.07
381.18	9.49	5.12
	Back Arc	
0.00	3.60	2.08
2.00	5.40	3.12
3.50	6.25	3.61
8.50	7.00	4.04
14.50	7.50	4.33
35.10	7.85	4.36
40.13	7.86	4.38
60.28	8.01	4.46
80.51	8.04	4.49
100.79	8.19	4.58
121.14	8.25	4.60
141.56	8.33	4.61
162.04	8.41	4.63
182.59	8.50	4.65
203.21	8.56	4.67
213.54	8.63	4.70
234.25	8.74	4.75
255.04	8.84	4.81
275.89	8.95	4.86
296.81	9.05	4.91
317.80	9.16	4.96
338.85	9.27	5.02
359.98	9.38	5.07
381.18	9.49	5.12
	South Shetland Platform	
0.00	3.60	2.08
2.00	4.70	2.71
3.50	5.30	3.06
5.00	6.20	3.58
13.00	6.95	4.01
25.00	7.50	4.33
35.10	7.85	4.36
40.13	7.86	4.38
60.28	8.01	4.46
80.51	8.04	4.49
100.79	8.19	4.58
121.14	8.25	4.60
141.56	8.33	4.61
162.04	8.41	4.63
182.59	8.50	4.65
203.21	8.56	4.67
213.54	8.63	4.70
234.25	8.74	4.75
255.04	8.84	4.81
275.89	8.95	4.86
296.81	9.05	4.91
317.80	9.16	4.96
338.85	9.27	5.02
359.98	9.38	5.07
381.18	9.49	5.12
	Antarctic Peninsula	
0.00	3.89	2.24
3.35	5.13	2.96
6.63	6.35	3.66
14.73	7.18	4.14
28.27	8.18	4.72
60.28	8.13	4.53
80.51	8.16	4.55
100.79	8.19	4.58
121.14	8.25	4.60
141.56	8.33	4.61
162.04	8.41	4.63
182.59	8.50	4.65
203.21	8.56	4.67
213.54	8.63	4.70
234.25	8.74	4.75
255.04	8.84	4.81
275.89	8.95	4.86
296.81	9.05	4.91
317.80	9.16	4.96
338.85	9.27	5.02
359.98	9.38	5.07
381.18	9.49	5.12

A. If the maximum radius was less than 5.2 km the quality was B, and if it was less than 10.5 km the quality was C. Events with a confidence ellipsoid spanning greater than 10.5 km from the location were considered quality D. We removed all of the C and D quality events from the data set, so all remaining earthquakes were located with a 95% confidence range of less than 5.2 km. We also observed that some earthquakes recorded only by land stations on the South Shetland Islands showed a high quality solution, yet the stations form a nearly linear array. In this case, the solution is nonunique and an additional high quality location may exist on the opposite side of the array. These earthquakes were also eliminated from the final data set. The resulting 122 quality A and 27 quality B events are shown in Figure 2, and the locations are listed in the auxiliary material.[1]

[18] The earthquake depth was more difficult to constrain accurately than lateral position, so we made a separate data set of earthquakes that have reliable depth estimates. We considered the depths to be well constrained if the location quality was A for the lateral location, the quality was A or B for the depth location, the earthquake was less than 75 km from the nearest station used in the location, and at least 8 arrivals were used in the location. This resulted in 50 earthquakes with reliable depth solutions; the results are plotted in Figure 4. A cross section of the same 50 events is shown in Figure 5.

3.1.4. Magnitude Calculation

[19] We used the method of *Veith and Clawson* [1972] to determine the magnitude of the earthquakes. We found that

[1] Supporting auxiliary material is available at ftp://agu.org/apend/jb/2003JB002416.

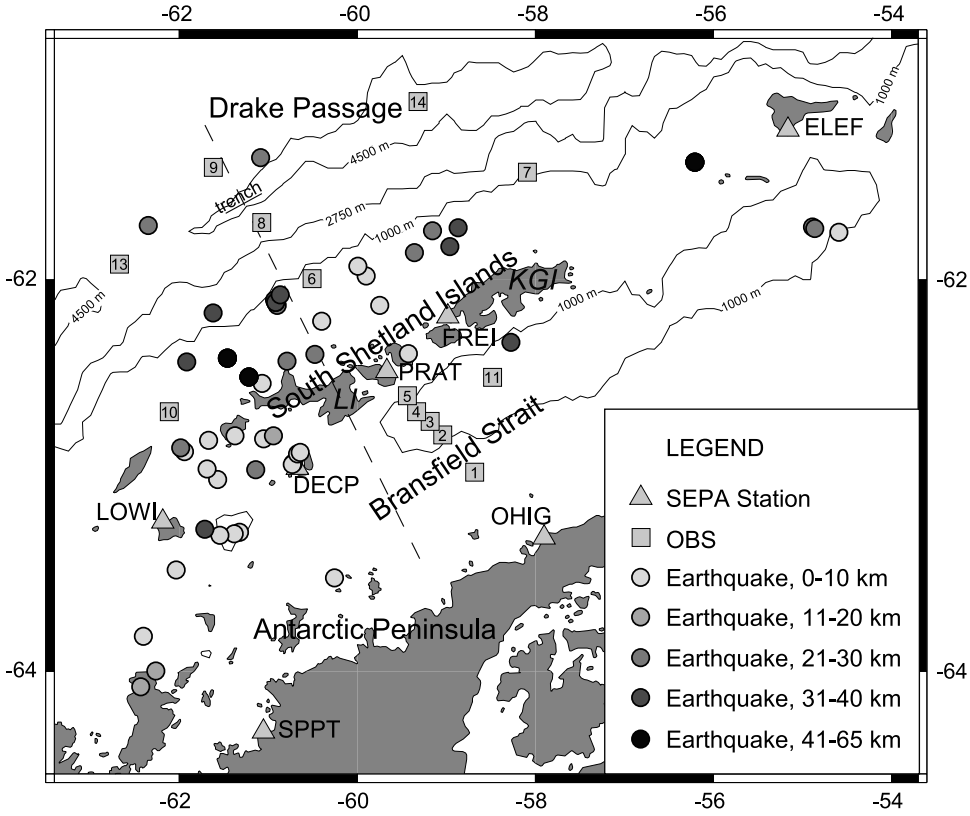

Figure 4. Events with well-constrained depth solutions. LI indicates Livingston Island, and KGI indicates King George Island. The events near the shallow thrust interface are 10–50 km deep. The events in the southwestern part of the back arc are shallow and probably related to new rifting or rotation about a near pole. The dashed line indicates the cross-section baseline shown in Figure 5.

12% of the events were in the range m_b = 2 to 3, 44% were in the range m_b = 3 to 4, and 37% were in the range of m_b = 4 to 5. 5% of the events had an m_b less than 2 or greater than 5. There is no previously established local magnitude scale in the South Shetland Islands region, but for the three events large enough to have International Data Center locations we found that the IDC m_b values agreed with our values within 0.1.

3.2. Focal Mechanisms

3.2.1. Waveform Inversion Method

[20] Although the earthquakes in this region are rather small, we were able to determine focal mechanisms for two of the larger events using regional waveform inversion. The high microseismic noise level, which peaks at 0.1–0.3 Hz, produced poor signal to noise ratios in that frequency range. In addition, at higher frequencies (0.3–1 Hz) the waveforms show a lot of scattered energy and are very sensitive to the local velocity structure, which is not known in detail. Several of the larger events were therefore inverted at frequencies of 0.025–0.07 Hz, a low-frequency range that is less sensitive to variations in the velocity structure and at which the seismograms have a higher signal to noise ratio.

[21] We first used a reflectivity code [*Kennett*, 1983] to calculate the synthetic seismograms for three fundamental focal mechanisms in the chosen frequency range. Synthetic seismograms can then be calculated for arbitrary focal mechanisms from a linear combination of these fundamental synthetic seismograms [*Langston and Helmberger*, 1975]. We used a grid search over fault strike, dip, slip, and time function duration to determine the focal mechanism and seismic moment with the lowest least squared misfit for the vertical and transverse waveforms.

3.2.2. The 19 February 1997 Event

[22] This event was located in a cluster of activity toward the northeast end of the Bransfield basin just south of Elephant Island and was one of the three local earthquakes recorded teleseismically during our deployment; it has a moment magnitude of M_w = 4.1. Several other events occurred on 19 February at essentially the same location, so this event represents the largest in a swarm of events on that day. The event is located at rather large distances from most of the stations and so the depth is not well resolved; because the Bransfield earthquakes are generally quite shallow we fixed the depth at 10 km. We used the back arc structure to calculate the synthetic seismograms for this event (Table 3). The solution uses seven waveforms at four stations, and is based largely on the fit to the combined shear wave and surface wave arrival (Figure 6). The resulting mechanism (strike 240, dip 45, slip 320) shows dominantly normal faulting with a small strike-slip component, and is consistent with extension at the axis of the Bransfield rift system.

3.2.3. The 27 January 1999 Event

[23] This event was located in the forearc at a depth of 33 km, ~60 km from the trench and 50 km from the coast of Livingston Island. M_w for this event is 4.6. We used a South Shetland platform velocity structure (Table 3) to calculate

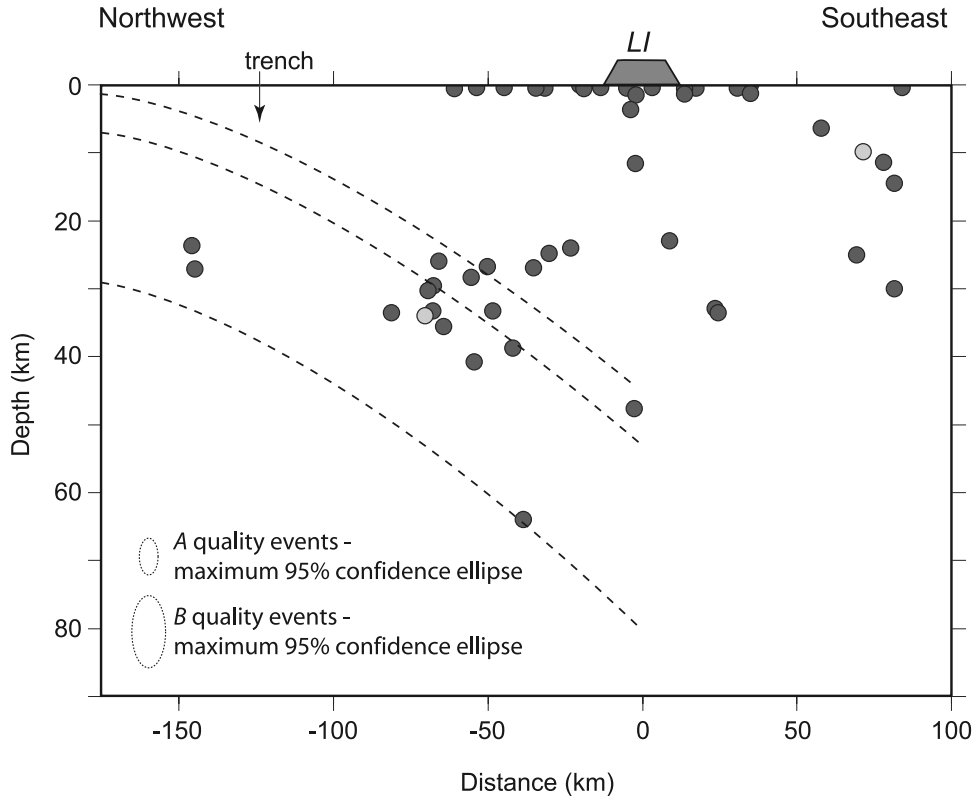

Figure 5. Cross section showing well-constrained depth solutions. The cross section goes through Livingston Island (LI) and is oriented perpendicular to the trench (see Figure 4 for orientation). The dashed lines indicate the possible location of the subducting slab (crust and lithosphere). The events for which focal mechanisms were calculated (Figure 6) are shown in light grey. The maximum sizes of the 95% confidence ellipsoids are indicated; they appear oblong due to the vertical exaggeration in the cross section. Note that all events shown in this cross section have a lateral quality of A.

the synthetic seismograms since both the event and most of the stations are located near the South Shetland Islands. The seven stations provide good azimuthal coverage and are generally well fit (Figure 6); this focal mechanism is better constrained than the 19 February 1997 event. The best fitting mechanism (strike 60°, dip 25°, slip 80°) shows a thrust faulting mechanism with a shallowly southeastward dipping plane that probably represents the fault plane. This mechanism is consistent with underthrusting of the oceanic Antarctic Plate beneath the South Shetlands microplate, and provides evidence for active convergence in the South Shetland trench.

[24] Figure 7 shows the two focal mechanisms described above as well as the Harvard Centroid Moment Tensor (CMT) solutions and locations for events from 1976 to 2002 http://www.seismology.harvard.edu/CMTsearch.html). The two events for which focal mechanisms were calculated are also indicated in the Figure 5 cross section.

4. Results and Discussion

[25] In contrast to the global records that indicate sparse seismicity in the South Shetland Island region, the data that we obtained from 1997 through 1999 indicate a high level of local seismicity (m_b 2–5). We have analyzed the 24 months of data during which the majority of the stations were working, and we were able to accurately locate almost 150 events (Figure 2). We also found many other events that were recorded only at one or two stations, or that had a nonunique location based on our station distribution, and were thus eliminated from our data set.

[26] Many of the earthquakes are located in the forearc region extending from the South Shetland trench axis toward and beneath the South Shetland Islands. This high level of activity suggests currently active convergence along the South Shetland subduction zone. The depths (generally 10–50 km) and locations of the earthquakes suggest they may represent the shallow thrust faulting events that generally occur along the shallowly dipping thrust interface of subduction zones. The focal mechanism for the 1/27/99 event confirms active thrust faulting occurs in the forearc. The maximum depth of earthquakes in this region appears to be ~65 km, suggesting there is no significant Wadati-Benioff zone extending into the mantle. The deepest earthquakes are located just seaward of the South Shetland Islands (Figures 4 and 5). The deepest event, located just off the coast of Livingston Island, was located using six stations and eight arrivals. The absence of a Wadati-Benioff zone is consistent with observations from other subduction zones involving slow subduction of very young lithosphere, such as Cascadia, the austral Andes, and Nankai [*Gutscher*, 2001; *Hyndman and Wang*, 1993; *Wang*, 2000]. The seismogenic zone is limited by a temperature above which the material deforms plastically. At the interface between a

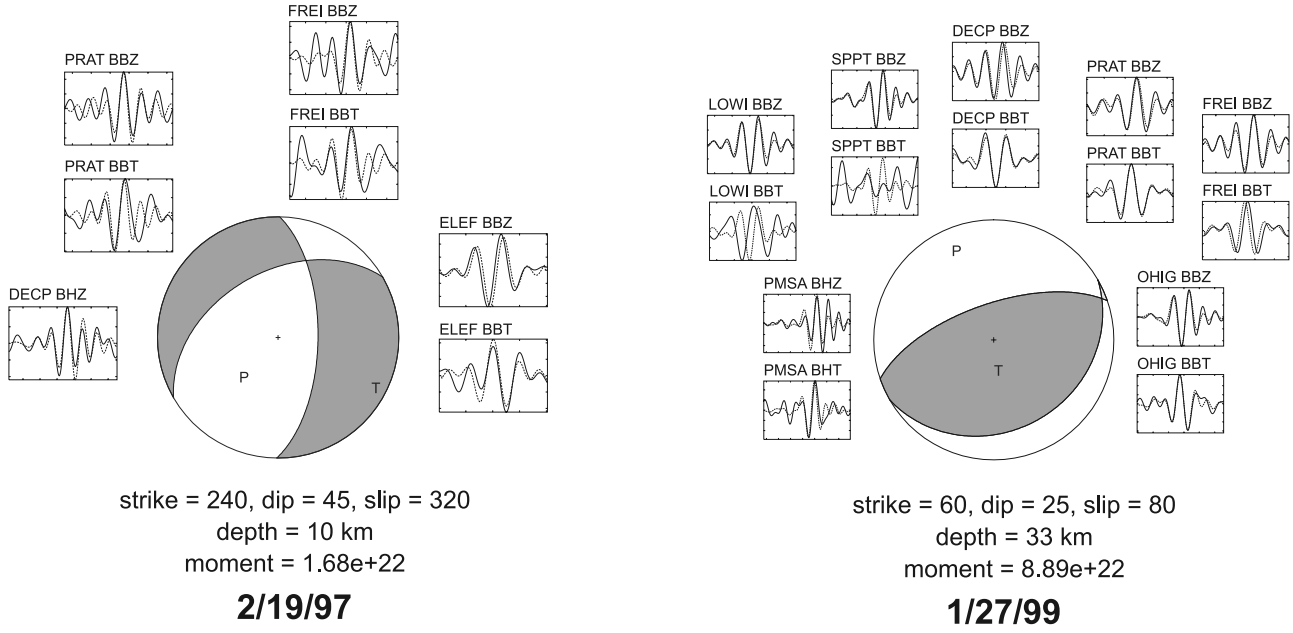

Figure 6. Focal mechanisms and waveform fits for two of the larger local earthquakes, 19 February 1997 and 27 January 1999. The solid lines represent the data, and the dotted lines represent the synthetic seismograms.

subducting slab and the overriding plate, the critical temperature beyond which seismic coupling does not occur is 400°C for lithosphere in contact with crustal material and 550°C for lithosphere in contact with mantle material [*Tichelaar and Ruff*, 1993]. For lithosphere not affected by a plate interface, seismicity generally ceases around 350–450°C for crustal rocks and at 800°C for mantle rocks [*Hyndman and Wang*, 1993; *Wiens and Stein*, 1983]. There-

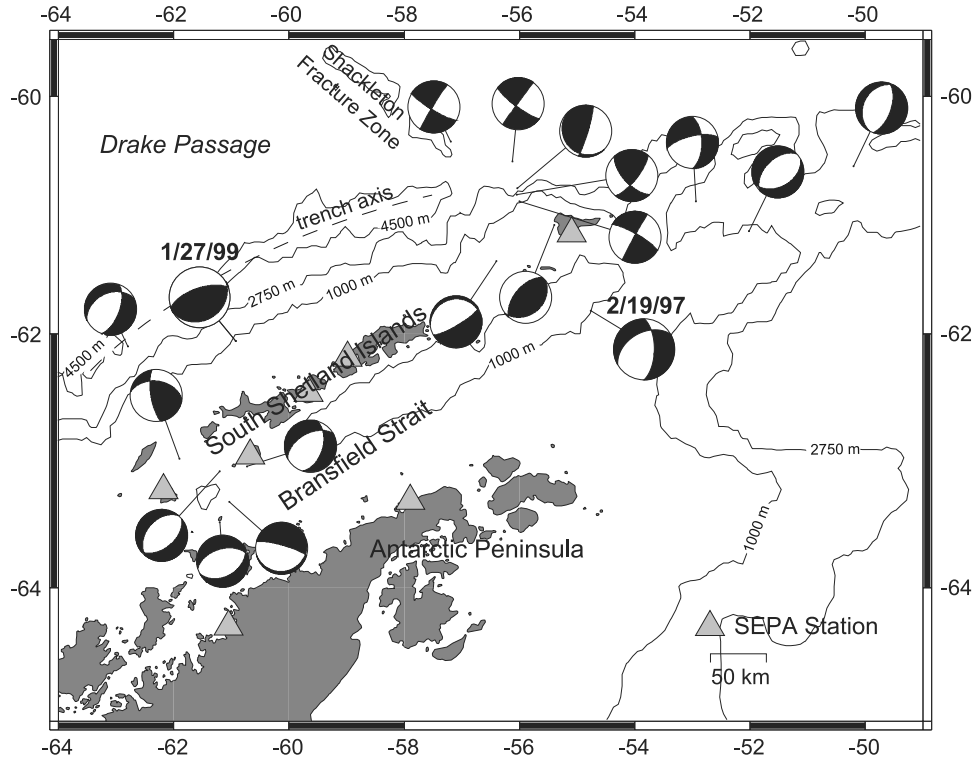

Figure 7. CMT focal mechanisms for events between 1976 and 2002 and the two focal mechanisms determined by local waveform inversion (19 February 1997 and 27 January 1999). The focal sphere sizes are not scaled by magnitude.

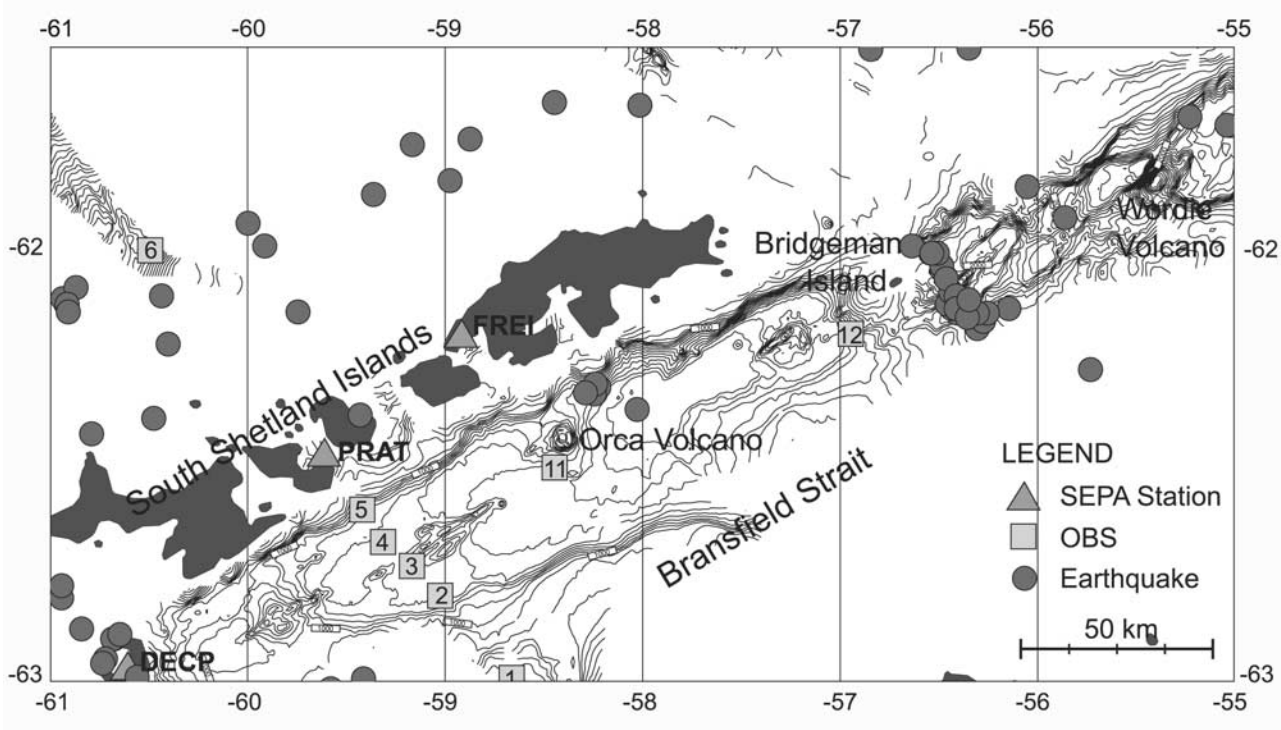

Figure 8. Earthquakes located in the central Bransfield Strait. A small group of earthquakes is located near Orca Volcano, perhaps indicating current magmatic or eruptive activity of this volcano. A large group of earthquakes is located near Bridgeman Island, where a rift is visible in the bathymetry. Bathymetry is from *Lawver et al.* [1996] and N. Kanjorski (unpublished data, 1999).

fore slabs can become aseismic before they are completely thermally assimilated into the mantle [*Severinghaus and Atwater*, 1991]. Young slabs and slowly subducting slabs will reach these transition temperatures at a shallower depth than older slabs or those subducting at a faster rate. Cascadia, the Austral Andes, Nankai, and the South Shetland Islands are all examples of slow subduction of young lithosphere. In the Cascades the subducting lithosphere is 8 Ma and subducts at a rate of 4 cm/yr. The lithosphere subducting beneath the South Shetland Islands is $\sim$14–23 Ma and subducts at a rate of 1 cm/yr. Although the subducting lithosphere in the South Shetland Island regions is older and cooler than that in the Cascades, it subducts more slowly and reaches high temperatures at shallow depths. The distribution of seismicity shown in Figure 5 is in fact similar to the distribution of seismicity in the Cascades [*Hyndman and Wang*, 1993].

[27] Many earthquakes are located in the back arc, either on large submarine volcanoes or along regions of rifting [*Gonzalez-Ferran et al.*, 1991]. Figure 8 shows a group of four earthquakes located on the northeastern flank of Orca Volcano. These events are relatively shallow and probably indicate continued activity, either magmatic or eruptive, at the submarine volcano. A large swarm of earthquakes is located on a well-established rift to the northeast of Bridgeman Island, with all hypocenters at depths of 12 km or less. Swarm seismicity is often associated with rifting and slow spreading centers. Indeed, many of these rift events occurred during short periods of time; six happened during one hour in 1999, and three events per hour occurred on several occasions in 1997. The seismic activity provides evidence of ongoing rifting, in agreement with petrological evidence, seafloor morphology, recent geodetic GPS results, and multichannel seismic reflection data [*Barker and Austin*, 1998; *Gamboa and Maldonado*, 1990; *Gracia et al.*, 1996; *Kim et al.*, 1995; *Larter and Barker*, 1991; *Maldonado et al.*, 1994].

[28] It is interesting to note that the earthquake distribution in Bransfield Strait is quite diffuse to the southwest of Deception Island, whereas the events to the northeast are strongly clustered (Figure 2). This distribution of events is consistent with bathymetric evidence suggesting the rifting is less well developed to the southwest, probably due to a smaller total cumulative extension. This could be caused either by rift propagation toward the southwest into continental crust which has undergone less extension [*Barker and Austin*, 1998], or by the rift opening about a near pole located to the southwest of Bransfield Strait [*Larter and Barker*, 1991]. These conclusions agree with bathymetric evidence that shows shallower depths and no clear rifting zones south of Deception Island. Further study of the spatial distribution and focal depths of earthquakes along the entire length of the Bransfield rift may provide important constraints on the mechanical processes involved in extension and rifting, and in particular the depth distribution of brittle faulting during different phases of rift development.

[29] There is fairly dense distribution of earthquakes near Low Island and just east of Smith Island. The Hero Fracture Zone intersects the South Shetland Platform at Smith Island, and its relationship to the South Shetland microplate may be the cause for some of this seismicity. If Antarctic plate material in Drake Passage is subducting beneath the

South Shetland Islands and rifting is occurring in the Bransfield Strait, the South Shetland microplate must be moving slowly northwest relative to the rest of the Antarctic plate. This motion would generate transcurrent faulting at the southernmost limit of the South Shetland microplate. However, seismic reflection profiles near the Hero Fracture Zone show no evidence of a sharp boundary between the active subduction zone to the northeast and the passive margin to the southwest [*Jin et al.*, 2002], so it is possible that the boundary between the two plates is diffuse and that the seismicity near Low Island and Smith Island is caused by uplift and the thermal effects resulting from interaction of the ridge crest with the margin near the Hero Fracture Zone.

[30] The overall level of seismicity is in the South Shetland region is consistent with other subduction zones showing slow subduction of very young oceanic lithosphere, such as Cascadia and the Southern Andes. Although global records indicated a low level of seismicity for the region and a lack of earthquakes seaward of the South Shetland Islands, the local SEPA deployment has enabled us to locate many earthquakes indicative of slow subduction. These earthquakes include probable subduction-related thrusting events, back arc rifting events, seismically active volcanoes, and transcurrent plate boundaries.

5. Conclusions

[31] The South Shetland Islands region displays many earthquakes (m_b 2–4) at locations and depths indicative of ongoing subduction. Earthquakes are located on both the outer rise and along the shallow thrust interface, and a focal mechanism for one of the larger events near the thrust interface confirms the presence of thrust faults. The maximum depth of seismicity is ~65 km, but the majority of the events are shallower than 30 km. These seismic results are consistent with recent GPS data that suggest a subduction rate of less than 1 cm/yr. Many earthquakes in Bransfield Strait are associated with volcanism and rifting. A group of events located on a submarine volcano suggests current magmatic activity, and swarms of events cluster along well-established rifts in the northeastern part of the Strait. The seismicity is much more diffuse to the southwest where the rifts are less established. This evidence supports the hypothesis that the back arc rift has opened more to the northeast than to the southwest, either due to propagation or rotation about a near pole.

[32] **Acknowledgments.** This experiment was supported by the Office of Polar Programs of the U.S. National Science Foundation under grants OPP9527366, OPP9725679, OPP9814622, OPP-9726180, and OCE9712900 and by the Instituto Antartico Chileno (INACH). The PASSCAL program of Incorporated Research Institutions in Seismology (IRIS) provided the seismological instrumentation. Allan Sauter adapted the PMD sensors for the OBSs. Stacey Robertson Maurice was supported by a National Science Foundation Graduate Fellowship. The data for the Esperanza station (ESPZ) were courtesy of Marino Russi, Alessandro Vuan, and Franco Arena at the OGS in Trieste, Italy; the station is managed by Italy and Argentina. Many people were involved in the deployment of these instruments. We would like to thank John Evans, Paul Friberg, Sergio Barrientos, Gonzalo Perez, Gideon Smith, Rodrigo Adaros, Kenneth Lein, Raul Rodriguez, and Eduardo Contreras for their assistance in the field, as well as the captains and the crews of the Chilean Naval vessel *Isaza* and the R/Vs *Abel J, Lawrence M. Gould*, and *Nathaniel B. Palmer*. We would also like to thank Nancy Kanjorski for her work with the bathymetry from the May 1999 Palmer cruise, and Rebecca Stiles, Maureen Langlois, Alice Diec, and Everett Criss for their assistance in processing the seismic data. Finally, we would like to thank Rob Larter and Alessandro Vuan for their helpful comments.

References

Ashcroft, W. A., Crustal structure of the South Shetland Islands and Bransfield Strait, *Br. Antarct. Surv. Sci. Rep.*, *66*, 43 pp., 1972.

Barker, D. H. N., and J. A. Austin, Crustal diapirism in Bransfield Strait, West Antarctica: Evidence for distributed extension in marginal basin formation, *Geology*, *22*, 657–660, 1994.

Barker, D. H. N., and J. A. Austin, Rift propagation, detachment faulting, and associated magmatism in Bransfield Strait, Antarcti Peninsula, *J. Geophys. Res.*, *103*(B10), 24,017–24,043, 1998.

Barker, D. H. N., G. L. Christenson, and J. A. Austin, Backarc basin evolution and cordilleran orogenesis: Insights from new ocean-bottom seismograph refraction profiling in Bransfield Strait, Antarctica, *Geology*, *31*, 107–110, 2003.

Barker, P. F., and I. W. D. Dalziel, Progress in geodynamics in the Scotia Arc region, in *Geodynamics of the Eastern Pacific Region, Caribbean and Scotia Arcs*, *Geodyn. Ser.*, vol. 9, edited by R. Cabre, pp. 137–170, AGU, Washington, DC, 1983.

Bevis, M., R. Smalley Jr., F. Taylor, and I. W. D. Dalziel, GPS studies of geodynamics in the Scotia Arc and West Antarctica, paper presented at 8th International Symposium on Antarctic Earth Sciences, Sci. Comm. on Antarct. Res., Wellington, New Zealand, 1999.

Cande, S. C., E. M. Herron, and B. R. Hall, The early Cenozoic tectonic history of the southeast Pacific, *Earth Planet. Sci. Lett.*, *57*, 63–74, 1982.

Cox, C. S., T. Deaton, and S. C. Webb, A deep-sea differential pressure gauge, *J. Atmos. Ocean. Technol.*, *2*, 237–246, 1984.

Della Vedova, B., Crustal structure and tectonic evloution of the northern Antarctic Peninsula, TENAP Seismic Experiment, paper presented at 8th International Symposium on Antarctic Earth Sciences, Sci. Comm. on Antarct. Res., Wellington, New Zealand, 1999.

Dietrich, R., et al., ITRF coordinates and plate velocities from repeated GPS campaigns in Antarctica—An analysis based on different individual solutions, *J. Geod.*, *74*, 756–766, 2001.

Forsyth, D. W., Fault plane solutions and tectonics of the South Atlantic and Scotia Sea, *J. Geophys. Res.*, *80*, 1429–1443, 1975.

Gamboa, L. A. P., and P. R. Maldonado, Geophysical investigations in the Bransfield Strait and in the Bellinghausen Sea-Antarctica, in *Antarctica as an Exploration Frontier: Hydrocarbon Potential, Geology, and Hazards*, edited by B. S. John, *AAPG Stud. Geol.*, *31*, 127–141, 1990.

Gonzalez-Ferran, O., J. A. Crame, and J. W. Thomson, The Bransfield Rift and its active volcanism, in *Geological Evolution of Antarctica*, edited by M. R. A. Thomson, J. A. Crame, and J. W. Thomson, pp. 505–509, Cambridge Univ. Press, New York, 1991.

Gracia, E., M. Canals, M. Li Farran, M. Jose Prieto, J. Sorribas, and G. Team, Morphostructure and evolution of the central and eastern Bransfield Basins (NW Antarctic Peninsula), *Mar. Geophys. Res.*, *18*, 429–448, 1996.

Gracia, E., M. Canals, M. L. Farran, J. Sorribas, and R. Pallas, Central and eastern Bransfield basins (Antarctica) from high-resolution swath-bathymetry data, *Antarct. Sci.*, *9*, 168–180, 1997.

Grad, M., A. Guterch, and T. Janik, Seismic structure of the lithosphere across the zone of subducted Drake plate under the Antarctic Plate, West Antarctica, *Geophys. J. Int.*, *115*, 586–600, 1993.

Grad, M., H. Shiobara, T. Janik, A. Guterch, and H. Shimamura, Crustal model of the Bransfield Rift, West Antarctica, from detailed OBS refraction lines, *Geophys. J. Int.*, *130*, 506–518, 1997.

Gutscher, M.-A., An Andean model of interplate coupling and strain partitioning applied to the flat subduction zone of SW Japan (Nankai Trough), *Tectonophysics*, *333*(1–2), 95–109, 2001.

Hyndman, R. D., and K. Wang, Thermal constraints on the zone of major thrust earthquake failure: The Cascadia Subduction Zone, *J. Geophys. Res.*, *98*, 2039–2060, 1993.

Ibanez, J. M., J. Morales, G. Alguacil, J. Almedros, R. Ortiz, and J. Del Pezzo, Intermediate-focus earthquakes under the South Shetland Islands (Antarctica), *Geophys. Res. Lett.*, *24*, 531–534, 1997.

Jacobson, R. S., L. M. Dorman, G. M. Purdy, A. Schultz, and S. C. Solomon, Ocean bottom seismometer facilities available, *Eos Trans. AGU*, *72*, 506, 511, 515, 1991.

Jin, Y. K., D. K. Lee, S. H. Nam, Y. Kim, and K. J. Kim, Seismic observation at King Sejong Station, Antarctic Peninsula, *Terra Antarct.*, *5*, 729–736, 1998.

Jin, Y. K., R. D. Larter, Y. Kim, S. H. Nam, and K. J. Kim, Post-subduction margin structures along Boyd Strait, Antarctic Peninsula, *Tectonophysics*, *346*, 187–200, 2002.

Jordan, T. H., and K. A. Sverdrup, Teleseismic location techniques and their application to earthquake clusters in the south-central Pacific, *Bull. Seismol. Soc. Am.*, *71*, 1105–1130, 1981.

Keller, R. A., M. R. Fisk, W. M. White, and K. Birkenmajer, Isotopic and trace element constraints on mixing and melting models of marginal basin volcanism, Bransfield Strait, Antarctica, *Earth Planet. Sci. Lett.*, *111*, 287–303, 1992.

Keller, R. A., M. R. Fisk, J. L. Smellie, J. A. Strelin, and L. A. Lawver, Geochemistry of back arc basin volcanism in Bransfield Strait, Antarctica: Subducted contributions and along-axis variations, *J. Geophys. Res.*, *107*(B8), 2171, doi:10.1029/2001JB000444, 2002.

Kennett, B. L. N., *Seismic Wave Propagation in Stratified Media*, 339 pp., Cambridge Univ. Press, New York, 1983.

Kennett, B. L. N., and E. R. Engdahl, Traveltimes for global earthquake location and phase identification, *Geophys. J. Int.*, *105*, 429–465, 1991.

Kim, Y., H.-S. Kim, R. D. Larter, A. Camerlenghi, L. A. P. Gambôa, and S. Rudowski, Tectonic deformation in the upper crust and sediments at the South Shetland Trench, in *Geology and Seismic Stratigraphy of the Atlantic Margin*, *Antarct. Res. Ser.*, vol. 68, edited by A. K. Cooper, P. T. Barker, and G. Brancolini, pp. 157–166, AGU, Washington, DC, 1995.

Lahr, J., HYPOELLIPSE: A computer program for determining local earthquake hypocentral parameters, magnitude, and first-motion pattern (Y2K compliant version), 1999 version 1.0, U.S. Geol. Surv., Reston,Va., 1999.

Langston, C. A., and D. V. Helmberger, A procedure for modelling shallow dislocation sources, *Geophys. J. R. Aston. Soc.*, *42*, 117–130, 1975.

Larter, R. D., Cenozoic tectonic history, seismicity, and palaeoseismicity of the Antarctic Peninsula Pacific margin, *Terra Antarct.*, *8*, 79–86, 2001.

Larter, R. D., and P. F. Barker, Effects of ridge crest-trench interaction on Antarctic-Phoenix spreading: Forces on a young subducting plate, *J. Geophys. Res.*, *96*, 19,583–19,607, 1991.

Lawver, L. A., B. J. Sloan, D. H. N. Barker, M. Ghedella, R. P. von Herzen, R. A. Keller, G. P. Kinkhammer, and C. S. Chin, Distributed active extension in Bransfield Basin, Antarctic Peninsula: Evidence from multibeam bathymetry, *GSA Today*, *6*(11), 1–6, 1996.

Maldonado, A., R. D. Larter, and F. Aldaya, Forearc tectonic evolution of the South Shetland margin, *Tectonics*, *13*(6), 1345–1370, 1994.

Nagihara, S., and L. A. Lawver, Heat flow measurements in the King George Basin, Bransfield Strait, *Antarct. J. U.S.*, *24*, 123–125, 1989.

Parra, J. C., and G. Yanez, Reconocimiento aeromagnetico en la peninsula Antartica y mares circundantes, integracion de informacion obtenida a diferentes alturas, *Ser. Cient. INACH*, *38*, 117–131, 1988.

Pelayo, A. M., and D. A. Wiens, Seismotectonics and relative plate motions in the Scotia Sea region, *J. Geophys. Res.*, *94*, 7293–7320, 1989.

Quinlan, D. M., D. Harvey, and G. Wagner, Datascope seismic application package, *Seismol. Res. Lett.*, *67*(2), 51, 1996.

Roach, P. J., The nature of back-arc extension in Bransfield Strait, *Geophys. J. R. Astron. Soc.*, *53*, 165, 1978.

Sauter, A. W., J. Hallinan, R. Currier, T. Barash, B. Wooding, A. Schultz, and L. M. Dorman, A new ocean bottom seismometer, in *Marine Instrumentation 1990*, pp. 99–104, Mar. Technol. Soc., Columbia, Md., 1990.

Severinghaus, J., and T. Atwater, Cenozoic geometry and thermal state of the subducting slabs beneath western North America, in *Basin and Range Extensional Tectonics Near the Latitude of Las Vegas*, edited by B. P. Wernicke, *Mem. Geol. Soc. Am.*, *176*, 1–22, 1991.

Tichelaar, B. W., and L. J. Ruff, Depth of seismic coupling along subduction zones, *J. Geophys. Res.*, *98*, 2017–2037, 1993.

Veith, K. F., and G. E. Clawson, Magnitude from short-period *P*-wave data, *Bull. Seismol. Soc. Am.*, *62*, 435–452, 1972.

Vuan, A., Joint inversion of receiver function of teleseismic body waves and local group velocity dispersion curves beneath ESPZ and PMSA stations (Antarctic Peninsula), *Terra Antarct.*, *8*, 49–54, 2001.

Wang, K., Seismic structure and stress regime of subduction zones; selected papers, *Tectonophysics*, *319*(4), 321–338, 2000.

Weaver, S. D., A. D. Saunders, R. J. Pankhurst, and J. Tarney, A geochemical study of magmatism associated with the initial stages of back-arc spreading: The Quaternary volcanics of Bransfield Strait, and South Shetland Islands, *Contrib. Mineral. Petrol.*, *68*, 151–169, 1979.

Wiens, D. A., and S. Stein, Age dependence of oceanic intraplate seismicity and implications for lithospheric evolution, *J. Geophys. Res.*, *88*, 6455–6468, 1983.

L. M. Dorman, Scripps Institution of Oceanography, University of California, San Diego, 9500 Gilman Drive, La Jolla, CA 92093-0220, USA. (ldorman@ucsd.edu)

S. D. Robertson Maurice, ExxonMobil Upstream Research Co., 3319 Mercer Street, Houston, TX 77027, USA. (stacey.d.maurice@exxonmobil.com)

P. J. Shore and D. A. Wiens, Department of Earth and Planetary Sciences, Washington University, One Brookings Drive, 1169, St. Louis, MO 63130, USA.

E. Vera, Departmento de Geofisica, Universidad de Chile, Santiago, Blanco Encalada 2085/Casilla, Santiago, 2777 Chile.